Journal of Computational Systems Biology
Volume 5 | Issue 1
ISSN: 2455-7625

Research Article Open Access

Computer Simulations of Brain Oxygenation at the Microvascular Level Validating a New Role of the Arterioles

Titovets E*

Department of Neurosurgery of Republican Research and Clinical Center of Neurology and Neurosurgery, Minsk, Belarus

***Corresponding author:** Titovets E, Department of Neurosurgery of Republican Research and Clinical Center of Neurology and Neurosurgery, Fr. Skoriny Str, 24, Minsk, Belarus, 220114, E-mail: eptitovets@gmail.com

Citation: Titovets E (2020) Computer Simulations of Brain Oxygenation at the Microvascular Level Validating a New Role of the Arterioles. J Comp Sys Bio 5(1): 101

Abstract

Brain physiology critically depends on constant oxygen supply to the neurons to ensure various energy–dependent functions of the central nervous system. A volume of latest experimental data on oxygen metabolism obtained with high temporal and spatial resolution, with both invasive and non-invasive methods, and the use of technologies of various degrees of sophistication, strongly suggests arteriole involvement in brain oxygenation. This new approach challenges the traditional views on brain oxygenation according to which oxygen supply to the brain tissues occurs by diffusion at the capillary level.

In this research, a computer simulation of brain oxygenation at the microvascular level has been carried out to assess the role of the arterioles in the process. The model is based on the convective nanofluidic (CNF) mechanism of brain water metabolism involved in oxygen mass-transfer [1,2]. The carried out simulations demonstrate that the arteriole oxygen supply dominates over the capillary oxygen delivery. The oxygen supply rates by arterioles can well meet the neuronal demands. The model accounts for some oxygen partial pressure (PO_2) distribution patterns in the brain that are hard to explain from the conventional capillary-oxygen-diffusion theory.

Keywords: Brain Oxygenation; Arterioles; Computational Model and Simulations; Convective Nanofluidic Mechanism

Introduction

Brain physiology critically depends on constant oxygen supply to the neurons to ensure various energy–dependent functions of the central nervous system. In energy terms, the brain accounts for over 20% of total body oxygen metabolism with the neurons consuming 75%–80% of the energy produced by the brain mitochondrial system [3]. The brain lacks any substantial energy reserve and entirely depends on the cerebral microcirculation, which responds quickly and locally to the metabolic needs of neurons via neurovascular coupling during neuronal activation [4-6].

Information on PO_2 distribution in the brain and PO_2 mapping is crucial for understanding cerebral oxygen metabolism and building any realistic model of brains oxygenation. PO_2 of the brain has been studied across species in some detail using technologies of various degree sophistication, with high temporal and spatial resolution, both invasive and non-invasive ones [7-15].

The reported values for PO_2 in the cerebral arteries are 91-124 mm Hg [16-18]. PO_2 in larger pial arterioles with the diameter equal or over 40 μm is above 100 mmHg decaying to about 65 mmHg in the 10-μm arterioles [18,19]. PO_2 in the capillaries is 25–35 mm Hg [11,16,18,20] and in the cortical venues is 33-44 mmHg [16,18,21].

A research on the radial profiles of tissue PO_2 around arterioles yielded some rather unexpected findings. The periarteriolar PO_2 in the pial microvessels in normoxia was ~99 mmHg in the vessels of 230 μm diameter and ~ 73 mmHg in the vessels of ~22 μm diameter [22]. Overall, the tissue PO_2 values were in the range of ~ 5–100 mm Hg, with the higher values occurring in regions close to pial arterioles [8,9,18,20,23]. The brain tissue PO_2 around capillaries is about 15 – 29 mmHg [17,24,25].

Non-invasive measurement of cerebrospinal fluid PO_2 in humans using MRI visualisation makes it possible to obtain absolute PO_2 quantification [26]. It shows that PO_2 in the CSF of the cortical sulci is 106 ± 42 mm Hg [7,21,27,28]. On inhalation pure oxygen it rises up to 248 ± 50 Hg [27]. Considered against the PO_2 of 25–35 mm Hg in the capillaries, it poses a question if the capillaries may be the only oxygen supply source to the tissue. There is also an obvious disagreement between the high PO_2 in the venules and low oxygen in the capillaries.

Rapid oxygen enhancement and the high PO_2 values in sulcal CSF have been interpreted as an indication of a possible direct transfer of O_2 from the pial arterioles into the CSF [15,16,29]. Based on the accumulated data a conclusion has been drawn that all microvessels, but not exclusively the capillaries, may supply oxygen to brain tissue [16,18,30,31]. Contribution of the arterioles in supplying brain tissues with oxygen is stressed. The new evidence challenges the common views of capillaries as the major site of O_2 delivery [18].

Oxygen supply by capillaries to the surrounding tissue is based on the Krogh's oxygen diffusion mechanism [32]. The controversy about the oxygen supply mechanism asks for a paradigm shift and the use of other approaches to look into the problem [1,33,34].

Brain microvessels are highly permeable to water. The most active water-conducting aquaporin AQP4, involved in regulation of water flux through the blood-brain barrier (BBB), is expressed in the astrocyte endfeet enveloping the microvessels. It ensures kinetic control over water movement between the blood and the brain interstitial space [35-40]. The walls of the cortical arterioles are permeable to oxygen [16,31].

The brain extracellular space (ECS), an intricate network of nanoslits and nanochannels, is a conduit for the extracellular fluid (ECF). The ECS presents a nanofluidic domain where fluid movement is governed by the slip-flow mechanism [41,42]. The ECF, a mobile medium, surrounds all neurons and other components of the brain parenchyma and may serve a vehicle for oxygen, energy substrates, information molecules etc. There is constant convective exchange between the CSF and the ECF [43]. It should be noted that according to the orthodox views, the ECS presents a diffusion barrier to mass transfer [44-46].

The aims of the present research has been to build a computer model of oxygen metabolism at the microvascular level, based on the CNF mechanism, and to explore its oxygen-mass-transfer capacity with a special attention given to the function of the arteriolar section.

Methods

We consider a simplified linear microvascular array consisting of a feeding arteriole, a capillary and a draining venule [47]. This structure is modelled as two right frustums joined at the top (Figure 1). Contrary to the oxygen diffusion models [48,49], no restrictions are imposed on the spatial arrangement of these microvessels in respect to the neurons. The geometric characteristics of the microvessels and other pertinent parameters for the model have been obtained from the literature [50,51].

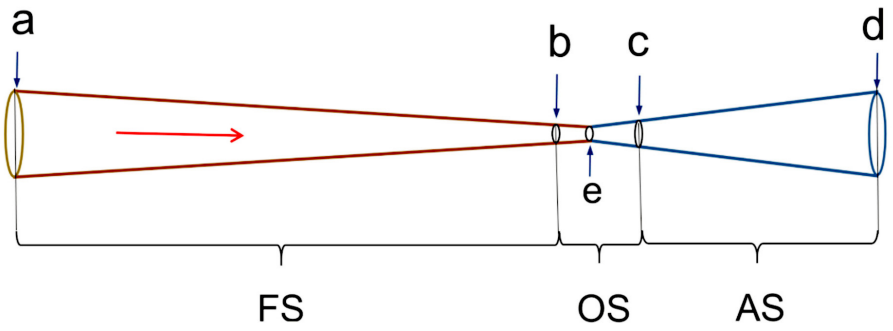

FS: the filtration section, between **(a)** and **(b)**; **OS**: the oscillatory section, between **(b)** and **(c)**; RS: the reabsorption section, between **(c)** and **(d)**. The blood flow proceeds from **(a)** to **(d)** as indicated by the arrow. The narrowest diameter in the system is at **(e)**. Anatomically it belongs to the capillary. The axial dimensions of each functional section have been computed.
Figure 1: Layout of the model microvascular array and its functional sections

For clarity of presentation, the diameters of the microvessels are rendered about thirty times larger compared to the overall length of the system.

The simulations have been carried out in two steps: (i) evaluation of the radial water volumetric flow rates and (ii) evaluation of the molar oxygen mass-transfer rates in consideration of the water volumetric flow rates, oxygen solubility and oxygen molar volume.

To model the radial water fluxes we used Kedem-Katchalsky formalism, based on linear non-equilibrium thermodynamics [52]:

$$J_v = L_p S\left(P_a - \Delta P x - f(t) - \pi_p + \pi_{ISF}\right), \quad (1)$$

where J_v, is the volumetric flow rate of water (cm^3/s/mmHg per cm^2 transfer area); L_p is an AQP4-dependent hydraulic conductivity coefficient (13.7 10^{-6} cm/s/mmHg) [1]; $S = LSA$ is the frustum lateral surface area (cm^2):

$$LSA = \pi(R+r)\sqrt{(R-r)^2 + L^2}, \quad (2)$$

where π = 3.14;
R and r are frustum radii (cm): **R > r**;
L is the frustum slant height (cm).
P_a is the hydrostatic pressure at a (66.6 mmHg).
ΔP is the axial hydrostatic pressure gradient (mmHg/cm):

$$\Delta P = (P_a - P_d) / L_{ad} \ , \tag{3}$$

Where P_a (mmHg) and P_d (mmHg) is the hydrostatic pressure at ***a*** and ***d***, respectively,
P_d is the venular hydrostatic pressure (6.6 mmHg);
L_{ad} is the overall length of the linear microvessel array (cm).
x is a distance from **a** (cm) at any point on the longitudinal axis of the microvessel array.
f (t) is an analytical form for the intracranial pressure (ICP) as a function of time (for the ICP pressure waveforms shown in Figure 2).
π_p is the plasma oncotic pressure (22 mmHg).
π_{ISF} is the interstitial fluid oncotic pressure (1 mmHg).

The overall fluid transfer between the blood and the interstitial fluid is isosmotic [36,53] driven by the hydrostatic pressure gradients between the blood and the surrounding tissue [54-56]. The volumes of water transferred in various sections of the model have been found by numerical integration of Eqn. 1.

The molar oxygen mass transfer rates, dO_2 / dt (fmol/min per LSA), have been obtained from:

$$dO_2 / dt = \alpha V_{H2O} S / V_m^{O2} \ , \tag{4}$$

where α is the Henry's law solubility constant (2.80 x 10^{-3} cm^3 O_2/cm^3 at 37 °C and 100 mmHg PO_2);
V_{H2O} is the volumetric flow rate of water (cm^3/ min);
$V_m^{O_2}$ is the molar volume of oxygen (193313 cm /mol at 37 °C and 100 mmHg PO_2).

The intracranial hydrostatic pressure (ICP) waveforms (Figure 2) have been digitized and approximated by analytical expressions using TableCurve. Computer simulations have been carried out using Mathematica 10 program and solved numerically [1,2].

Results

The spatiotemporal presentation of our simulation results reveals some interesting features about water metabolism in the microvascular system (Figures 2 and 3). The interplay of the hydrostatic and the oncotic pressure gradients outside of and inside the microvessels results in establishing distinct water flux patterns along the length of the microvascular array. Such patterns has been demonstrated in our earlier research on the brain water metabolism and the capillary water exchange [1]. Our present simulation, encompassing microvessels beyond exclusively capillary area, demonstrate different quantitative results.

Figure 2 shows water movement in the filtration and the reabsorption segments of the microvessels.

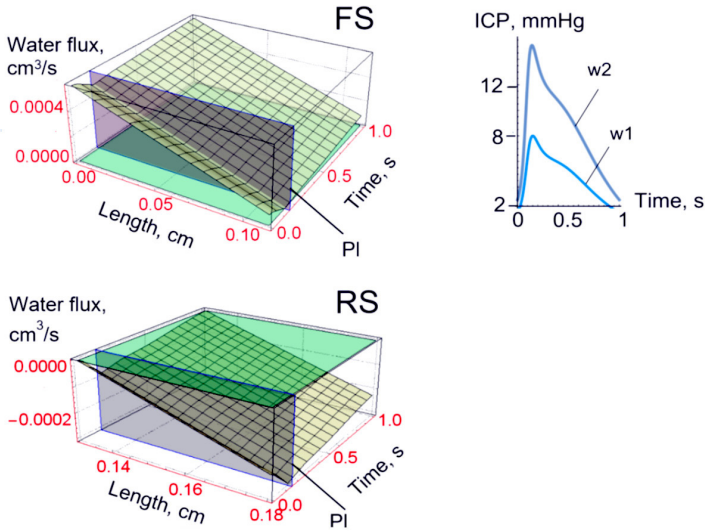

FS: filtration section; **RS:** reabsorption section; **Pl:** infinite plane passing through the minimum at 0.14 s
In the right top corner, there are the two ICP waveforms used in current simulations, **w1** and **w2**, with the maxima 8 mmHg and 15 mmHg, respectively. The wave's frequency is 1 Hz. The axial dimension of the FS is 0.12 cm. The FS presents a functional division of the microvascular system. Anatomically it includes the arteriole and part of the capillary. The hydrodynamic pressure at the arterial end of the arteriole is set at 66.6 mmHg (Table 1).
Figure 2: Water movement in the filtration and the reabsorption sections of the microvascular array

No	Feeding arteriole diameter at **a**, cm x 10^{-4}	Hydrostatic pressure at **a**, mmHg	ICP wave max/ min, mmHg	LSA, cm^2 x 10^{-4}	Radial water flux, cm^3/min x 10^{-6}	Oxygen supply rate in normoxia†, fmol /min	Oxygen supply rate in hyperoxia ††, fmol /min
1	40	66	*8.0/ 2.0	9.3	1.86	26.9	64.8
2	60	66	*8.0/ 2.0	12.6	2.52	34.5	83.1
3	80	66	*8.0/ 2.0	16.3	3.26	47.3	114.0
4	80	66	**15.0/ 2.9	15.0	2,40	34.8	83.9

*Wave **w1**; **Wave **w2**; †Respiration with 21% oxygen; ††Respiration with 95% oxygen
Table 1: Parameters of water movement and oxygen supply rate within the FS in the microvascular array

To simulate the effects of the changes in the volumetric blood flow on the radial water flux, the entrance diameter of the feeding arteriole was set to 40 μm, 60 μm and 80 μm. Table 1 demonstrates corresponding increases in the radial water flux and oxygen supply rates with the diameters.

An increase in the ICP (wave **w2**) results in a decrease of the radial water flux and the oxygenation rate.

With the axial dimension 0.0605 cm and the venule outlet diameter 60 μm, the RS reabsorbs about 14% of the filtrated water. The rest of the filtrated water gets into the ECF and, moving along the nanodimentional ECS, schould be reabsorbed into either other venules or mix, eventually, with the bulk CSF.

On normobaric inhalation of 95% oxygen there is observed a considerable increase of oxygen partial pressure in the microvessels and surrounding tissues reaching 241 mHg O2 in arterioles 30 μm diameter [31]. This is translated into a 2.41- times increase in the oxygen supply rate by the CNF mechanism.

In Figure 3 there are presented results on water exchange within the oscillatory section of the microvascular system.

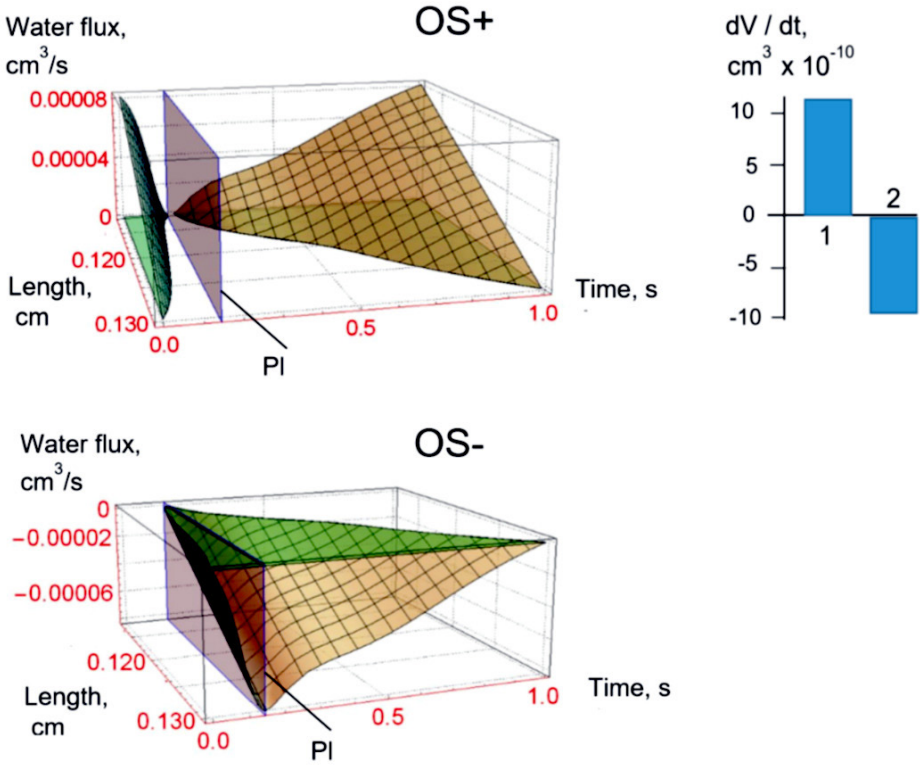

OS+ presents the filtrated water and **OS-** the reabsorbed water. **Pl** indicates the infinite plane passing through the minimum at 0.14 s. The bar graph in the right top corner presents the volumes of the filtrated (1) and the reabsorbed (2) water over a complete cardiac cycle.
Figure 3: Simulation results on water movement in the oscillatory section of the microvascular system

Compared to the FS, the radial water fluxes within the OS are low. As has been suggested before, the oscillatory pattern of water fluxes in the OS, as shown by the bar graph, facilitates fast informational exchange between the brain and the systemic blood [1]. The frequency of this exchange is controlled by the heart beat rate.

Discussion

A large body of evidence and experimental results on oxygen partial pressure distribution in the brain challenges the capillary oxygen diffusion theory of brain oxygenation. It asserts that the arterioles may play a key role in oxygen supply to the cerebral tissue [16,18,30,31,57] This controversy directly touches upon the mechanisms of brain oxygenation.

In our simulations, we employed a simple linear microvascular array of an arteriole, a capillary and a venule to investigate the extent of involvement of a particular arteriolar section in the oxygen exchange. The model is based on the CNF mechanism of brain water metabolism engaged in oxygen mass transfer in the brain tissues [1,2].

Our results demonstrate that the arteriole section of the array presents the main source of oxygen supply. The obtained oxygen supply rates of 26.9 - 47.3 fmol/min, in normoxia, and 64.8 - 114.0 fmol/min, in hyperoxia, are well compared with the oxygen consumption rate by an average neuron of the human brain, 27.4 fmol/cell/min [58], and by an average neuron of the brain across species, 0.66 - 60.0 fmol/cell/min [58,59].

In this research, we concentrated only on small-diameter arterioles. There is evidence that larger arterioles may equally supply oxygen to the surrounding tissues [16,18,30,31,60]. Considering all that, one may well assume that within the arteriolar networks there would be even higher oxygen supply rates compared to those obtained on a simple microvascular system under study in this paper.

Our earlier simulations carried out on a capillary model give oxygen supply rate of 0.88 fmol/min [2]. The arteriolar rates are thus 30 - 53 times higher than the capillary ones. This underscores the metabolic importance of arterioles in brain oxygenation.

Oxygen supply rate increases with an increase of the arteriole diameter (Table 1). Considered from the point of views of the regulation mechanism of neuronal oxygen-supply, it demonstrates the way the changes in the arteriole diameter influence the oxygen supply rates. This effect is observed in the neurovascular coupling, as a response to the neuronal activation [4-6,61,62].

Increasing intracranial hydrostatic pressure negatively reflects on brain oxygenation (Table 1, wave 2). It might serve as an early indication to the effect of a moderate increase of the ICP on brain energy metabolism.

A commonly accepted brain oxygenation mechanism is based on the oxygen diffusion theory put forward by Krogh where the flow of oxygen in the tissue is driven by a concentration gradient of oxygen between the blood to the cells [48,63]. Diffusion mechanism intrinsically sets limits for the critical radius of 30 to 40 μm around a capillary within which sufficient oxygenation of the tissue is only possible [64]. There are other limitations of diffusion when applied to the brain [59]. The spatial organization of the vascular system where oxygen content is higher than in tissue, is a key factor for maintaining effective oxygen supply [65]. Contrary to diffusion, the CNF mechanism of brain oxygenation is free of distance limitations or restrictions on spatial organization [1,2].

There are some observations that are difficult to explain by the oxygen diffusion mechanism alone operating at the capillary level [66-68]. For example, PO_2 in the outflowing blood of the cortical venules is higher than in the capillaries [16]. It is by 39% higher in the CSF than in the venous blood [14]. PO_2 in the sulcal CSF is close or equal to that in the arterial blood and from 4 to 5 times higher than in the capillary blood [27].

To cope with this situation we have put forward a conceptual view of a convective extracapillary transfer of oxygen [68,69] and further explored this issue within a nanofluidic approach to brain water metabolism [1,2,70].

Extremely energy demanding neural activity is coupled to the mitochondrial energy production and critically depends on tissue oxygenation [71,72]. The local oxygen consumption rates, depending on the neuronal activity, may change by a factor of about five [64]. Monitoring the redox-state of the components of the mitochondrial electron transfer chain makes it possible to closely study respiratory functions of the mitochondria, both *in vitro* and *in vivo* [73]. The intensity of mitochondrial respiration is commonly assessed on the basis of the NAD+/NADH ratio [74].

In our earlier research, we studied, in an open-system device, the NAD+/NADH ratio in mitochondria under the controlled oxygen supply rates. The zero-order kinetics of the oxygen consumption rates by the mitochondria continued down to the critical $PO_2 \approx$ I mm Hg. Below that value, the mitochondria entered the controlled hypoxic states characterized by uncoupling of oxidative phosphorylation the extent of which depended on the level of the hypoxia. The hypoxic uncoupling was fully reversed on return to normoxia. [75-77].

NADH fluorescence imaging has been used to study *in vivo* the effect of AQP4 deletion on oxygen microdistribution. Deletion of Aqp4 increases NADH fluorescence, a sign of tissue hypoxia, in the areas furthest away from cerebral microvessels. This, for the first time, clearly demonstrates AQP4 participation in the oxygen supply [78]. The fact that AQP4 deletion manifests itself furthest away from the cerebral microvessels excludes the diffusion mechanism of oxygen transport with its critical oxygenation radius. At the same time, it fully agrees with functioning of the CNF mechanism of brain oxygenation.

The CNF mechanism explains the enhancement of the venular PO_2. Indeed, in the microvascular arrangement under study, the venular RS reabsorbs 14% of the water filtrated in the FS. This flux carries oxygen to the venule thus increasing the PO_2 in the outflowing blood.

The steady–state level of PO_2 in the sulcal CSF of about 106 mmHg is notably high and at least 3-4 times over that of the capillary PO_2 [21,27]. The subpial zone is characterized by the absence of capillary vessels [79]. High oxygen consumption by the surrounding tissue asks for equally high oxygen supply rate to maintain a steady-state level of PO_2. In this situation, the capillaries are unlikely oxygen suppliers by the diffusion mechanism. It is the pial arteriolar network, with the walls of arterioles permeable to oxygen, that presents a most probable source of oxygen for the sulcal CSF [16,22,80]. The close values of PO_2 in both the arterioles and the CSF would further preclude a fast oxygen supply rate by diffusion. Oxygen supply there may be realized through the CNF mechanism instead.

The computational model of brain oxygenation, based on the CNF mechanism, demonstrates a good oxygen-supply capability for the arterioles. Within the framework of this model there are found explanations for the experimental observations on the arteriolar involvement in oxygen supply including those results that are difficult or impossible to explain within the conventional capillary diffusion theory.

Conclusion

Brain function critically depends on continuous oxygen supply by the bloodstream. A commonly accepted view on brain oxygenation centers on the capillaries as the main source of oxygen for the brain tissues.

The progress in the technology of oxygen assessment and mapping in the brain, along with the new accumulated experimental data, challenge the exclusive role of the capillaries in brain oxygenation and suggests the arterioles as an alternative source of oxygen.

Carried out computer simulations of brain oxygenation demonstrate that the arterioles present an important source of oxygen for the neurons dominating over the capillary supply. Contrary to the diffusion-based orthodox theory, oxygen mass transfer is realized through the CNF mechanism of brain water metabolism [1,33]. The simulations account for the 'anomalous' oxygen partial pressure distribution in the brain tissues and the increase of oxygen in the outflowing venous blood, the observations that are difficult to explain from the conventional capillary-oxygen-diffusion theory. The simulations underscore the important role of the arterioles in brain oxygenation.

Acknowledgement

The author acknowledges financial support from the National Academy of Sciences of Belarus through grant 3.09-2016-20 of State Research Programme "Convergency-2020".

Conflict of Interest Declaration

The author declares no competing financial interests.

References

1. Titovets E (2018) Novel Computational Model of the Brain Water Metabolism: Introducing an Interdisciplinary Approach. J Comp Biol Sys 2: 1-11.

2. Titovets E (2019) Computer Modeling of Convective Mass Transfer of Glucose, Oxygen and Carbon Dioxide in the Neurovascular Unit. J Comp Biol Sys 4: 1-8.

3. Hyder F, Rothman DL, Bennett MR (2013) Cortical energy demands of signaling and nonsignaling components in brain are conserved across mammalian species and activity levels. Proc Natl Acad Sci USA 110: 3549-54.

4. Smith A, Doyeux V, Berg M, Peyrounette M, Haft-Javaherain M, et al. (2019) Brain Capillary Networks Across Species: A few Simple Organizational Requirements Are Sufficient to Reproduce Both Structure and Function. Front Physiol 10: 233.

5. Hillman EM (2014) Coupling mechanism and significance of the BOLD signal: a status report. Annu Rev Neurosci 37: 161-81.

6. Rungta RL, Chaigneau E, Osmanski BF, Charpak S (2018) Vascular Compartmentalization of Functional Hyperemia from the Synapse to the Pia. Neuron 99: 362-75.

7. Finikova O, Lebedev A, Aprelev A (2008) Oxygen microscopy by two-photon-excited phosphorescence. Chemphyschem 9: 1673-9.

8. Lyons D, Parpaleix A, Roche M, Charpak S (2016) Mapping oxygen concentration in the awake mouse brain. Elife 2016: 10.7554/eLife.12024.

9. Devor A, Sakadzic S, Saisan PA, Yaseen MA, Roussakis E, et al. (2011) "Overshoot" of O2 is required to maintain baseline tissue oxygenation at locations distal to blood vessels. J Neurosci 31: 13676-81.

10. Parpaleix A, Houssen Y, Charpak S (2013) Imaging local neuronal activity by monitoring PO2 transients in capillaries. Nat Med 19: 241-6.

11. Ortiz-Prado E, Natah S, Srinivasan S, Dunn JF (2010) A method for measuring brain partial pressure of oxygen in unanesthetized unrestrained subjects: the effect of acute and chronic hypoxia on brain tissue PO2. J Neurosci Methods 193: 217-25.

12. Ndubuizu O, LaManna JC (2007) Brain tissue oxygen concentration measurements. Antioxid Redox Signal 9: 1207-19.

13. Gagnon L, Smith AF, Boas DA, Devor A, Secomb TW, et al. (2016) Modeling of Cerebral Oxygen Transport Based on In vivo Microscopic Imaging of Microvascular Network Structure, Blood Flow, and Oxygenation. Front Comput Neurosci 10: 1-20.

14. Finikova O, Troxler T, Senes A, DeGrado WF, Hochstrasser RM, et al. (2007) Energy and Electron Transfer in Enhanced Two-Photon-Absorbing Systems with Triplet Cores. J Phys Chem A 111: 6977-90.

15. Halmagyi DFJ, Gillett DJ (1967) Cerebrospinal fluid oxygen tension at different levels of oxygenation. Respir Physiol 2: 207-12.

16. Vovenko E (1999) Distribution of oxygen tension on the surface of arterioles, capillaries and venules of brain cortex and in tissue in normoxia: an experimental study on rats. Eur J Physiol 437: 617-23.

17. Maas AIR, Fleckenstein W, Jong DA, Santbrink H (1993) Monitoring Cerebral Oxygenation: Experimental Studies and Preliminary Clinical Results of Continuous Monitoring of Cerebrospinal Fluid and Brain Tissue Oxygen Tension. Monitoring of Cerebral Blood Flow and Metabolism in Intensive Care 59: 50-57.

18. Sakadzic S, Mandeville ET, Gagnon L, Musacchia J, Yaseen MA, et al. (2014) Large arteriolar component of oxygen delivery implies a safe margin of oxygen supply to cerebral tissue. Nat Commun 5: 5734.

19. Kazemi H, Klein RC, Turner FN, Strieder D (1968) Dynamics of oxygen transfer in the cerebrospinal fluid. Respir. Physiol 4: 24-31.

20. Sakadzic S, Roussakis E, Yaseen MA, Mandeville ET, Srinivasan VJ, et al. (2010) Two-photon high-resolution measurement of partial pressure of oxygen in cerebral vasculature and tissue. Nat Methods 7: 755-9.

21. Zaharchuk G, Busse RF, Rosenthal G, Manley GT, Glenn OA, et al. (2006) Noninvasive oxygen partial pressure measurement of human body fluids in vivo using magnetic resonance imaging. Acad Radiol 13: 1016-24.

22. Duling BR, Kuschinsky W, Wahl M (1979) Measurements of the Perivascular PO2 in the Vicinity of the Pial Vessels of the Cat. Pflugers Arch 383: 29-34.

23. Ortiz-Prado E, Dunn J, Vasconez J, Castillo D, Viscor G (2019) Partial pressure of oxygen in the human body: a general review. Am J Blood Res 9: 1-14.

24. Carreau A, El Hafny-Rahbi B, Matejuk A, Grillon C, Kieda C (2011) Why is the partial oxygen pressure of human tissues a crucial parameter? Small molecules and hypoxia. J Cell Mol Med 15: 1239-53.

25. Lucker A, Weber B, Jenny P (2015) A dynamic model of oxygen transport from capillaries to tissue with moving red blood cells. Am J Physiol Heart Circ Physiol 308: H206-16.

26. Zaharchuk G, Busse R, Rosenthal G, Manley GT, Dillon WP, et al. (2005) In vivo oxygen partial pressure measurement of human body fluids. Proc Intl Soc Mag Reson Med 13: 66.

27. Zaharchuk G, Martin AJ, Rosenthal G, Rosenthal G, Manley GT, et al. (2005) Measurement of cerebrospinal fluid oxygen partial pressure in humans using MRI. Magn Reson Med 54: 113-21.

28. Silver I, Erecińska M (1998) Oxygen and Ion Concentrations in Normoxic and Hypoxic Brain Cells. Adv Exp Med Biol 454: 7-16.

29. Mehemed TM, Fushimi Y, Okada T, Yamamoto A, Kanagaki M, et al. (2014) Dynamic oxygen-enhanced MRI of cerebrospinal fluid. PLoS One 9: e100723.

30. Vovenko E, Chuikin A (2010) Tissue Oxygen Tension Profiles Close to Brain Arterioles and Venules in the Rat Cerebral Cortex during the Development of Acute Anemia. Neurosci Behav Physiol 40: 723-31.

31. Ivanov KP, Sokolova IB, Vovenko EP (1999) Oxygen transport in the rat brain cortex at normobaric hyperoxia. Eur J Appl Physiol 80: 582-7.

32. Mintun MA, Lundstrom BN, SnyderAZ, Vlassenko AG, Shulman GL, et al. (2001) Blood flow and oxygen delivery to human brain during functional activity: Theoretical modeling and experimental data. Proc Natl Acad Sci USA 98: 6859-64.

33. Titovets E (2019) Mass-Transfer Events in the Nanofluidic Domain of the Brain Interstitial Space: Paradigm Shift. JGCB 2: 112-4.

34. Titovets E (2019) Nanofluidic Approach to Brain Water Metabolism. ANNR 1: 49-56.

35. Nagelhus EA, Ottersen OP (2013) Physiological roles of aquaporin-4 in brain. Physiol Rev 93: 1543-62.

36. Igarashi H, Tsujita M, Kwee IL, Nakada T (2014) Water influx into cerebrospinal fluid is primarily controlled by aquaporin-4, not by aquaporin-1: 17O JJVCPE MRI study in knockout mice. Neuroreport 25: 39-43.

37. Desai B, Hsu Y, Schneller B, Hobbs JG, Mehta AI, et al. (2016) Hydrocephalus: the role of cerebral aquaporin-4 channels and computational modeling considerations of cerebrospinal fluid. Neurosurg Focus 41: 10.3171/2016.7.FOCUS16191.

38. Brinker T, Stopa E, Morrison J, Klinge P (2014) A new look at cerebrospinal fluid circulation. Fluids and Barriers of the CNS 11: 10.

39. Mestre H, Hablitz LM, Xavier AL, Feng W, Zou W, et al. (2018) Aquaporin-4-dependent glymphatic solute transport in the rodent brain. Elife 2018: 10.7554/eLife.40070.

40. Wardlaw JM, Benveniste H, Nedergaard M, Zlokovic, BV, Mestre H, et al. (2020) Perivascular spaces in the brain: anatomy, physiology and pathology. Nat Rev Neurol 16: 137-53.

41. Abgrall P, Nguyen N-T (2009) Nanofluidics, Artech House, USA.

42. Godin AG, Varela JA, Gao Z, Danné N, Dupuis, JP, et al. (2017) Single-nanotube tracking reveals the nanoscale organization of the extracellular space in the live brain. Nat Nanotechnol 12: 238-43.

43. Xie L, Kang H, Xu Q, Chen MJ, Liao Y, et al. (2013) Sleep drives metabolite clearance from the adult brain. Sci 342: 373-7.

44. Nicholson C, Kamali-Zare P, Tao L (2011) Brain Extracellular Space as a Diffusion Barrier. Comput Vis Sci 14: 309-25.

45. Kamali-Zare P, Nicholson C (2013) Brain Extracellular Space: Geometry, Matrix and Physiological Importance. Basic Clin Neurosci 4: 282-6.

46. Sykova E, Nicholson C (2008) Diffusion in brain extracellular space. Physiol Rev 88: 1277-340.

47. Hudetz AG, Conger KA, Halsey JH, Pal M, Dohan O, et al. (1987) Pressure Distribution in the Pial Arterial System of Rats Based on Morphometric Data and Mathematical Models. J Cereb Blood Flow Metab 7: 342-55.

48. Krogh A (1919) The number and distribution of capillaries in muscles with calculations of the oxygen pressure head necessary for supplying the tissue. J Physiolo 52: 409-15.

49. Goldman D (2008) Theoretical models of microvascular oxygen transport to tissue. Microcirculation 15: 795-811.

50. Lapi D, Marchiafava PL, Colantuoni A (2008) Geometric characteristics of arterial network of rat pial microcirculation. J Vasc Res 45: 69-77.

51. Linninger AA, Xenos M, Sweetman B, Ponkshe S, Guo X, et al. (2009) A mathematical model of blood, cerebrospinal fluid and brain dynamics. J Math Biol 59: 729-59.

52. Friedman M (1987) Principles and Models of Biological Transport. J Biomech Eng 109: 179.

53. Oldendorf WH (1970) Measurement of brain uptake of radiolabeled substances using a tritiated water internal standard. Brain Res 24: 372-6.

54. Kao YH, Guo WY, Liou AJ, Chen TY, Huang CC, et al. (2013) Transfer function analysis of respiratory and cardiac pulsations in human brain observed on dynamic magnetic resonance images. Comput Math Methods Med 2013: 1-7.

55. Wagshul M, Chen J, Egnor M, McCormack E, Roche P (2006) Amplitude and phase of cerebrospinal fluid pulsations: experimental studies and review of the literature. J Neurosurg 104: 810-9.

56. Wagshul M, Eide P, Madsen J (2011) The pulsating brain: A review of experimental and clinical studies of intracranial pulsatility. Fluids Barriers CNS 8: 1-23.

57. Ivanov K, Sokolova IB, Vovenko EP (1999) Oxygen transport in the rat brain cortex at normobaric hyperoxia. Eur J Appl Physiol 80: 582-7.

58. Herculano-Houzel S (2011) Scaling of brain metabolism with a fixed energy budget per neuron: implications for neuronal activity, plasticity and evolution. PLoS One 6: e17514.

59. McMurtrey J (2016) Analytic Models of Oxygen and Nutrient Diffusion, Metabolism Dynamics, and Architecture Optimization in Three-Dimensional Tissue Constructs with Applications and Insights in Cerebral Organoids. Tissue Eng Part C: ME 22: 221-49.

60. Vovenko E (1999) Distribution of oxygen tension on the surface of arterioles, capillaries and venules of brain cortex and in tissue in normoxia: an experimental study on rats. Pflügers Archiv 437: 617-23.

61. Lorthois S, Cassot F, Lauwers F (2011) Simulation study of brain blood flow regulation by intra-cortical arterioles in an anatomically accurate large human vascular network: Part I: methodology and baseline flow. Neuroimage 54: 1031-42.

62. Xu HL, Pelligrino DA (2007) ATP release and hydrolysis contribute to rat pial arteriolar dilatation elicited by neuronal activation. Exp Physiol 92: 647-51.

63. Krogh A (1919) The rate of diffusion of gases through animal tissues, with some remarks on the coefficient of invasion. J Physiol 52: 391408.

64. Huchzermeyer C, Berndt N, Holzhutter HG, Kann O (2013) Oxygen consumption rates during three different neuronal activity states in the hippocampal CA3 network. J Cereb Blood Flow Metab 33: 263-71.

65. Masamoto K, Tanishita R (2009) Oxygen Transport in Brain Tissue. J Biomec Eng 131: 1-6.

66. Croci M, Vinje V, Rognes M (2019) Uncertainty quantification of parenchymal tracer distribution using random diffusion and convective velocity fields. Fluids Barriers CNS 16: 32.

67. Schey KL, Petrova RS, Gletten RB, Donaldson PJ (2017) The Role of Aquaporins in Ocular Lens Homeostasis. Int J Mol Sci 18: 1-17.

68. Titovets E (2007) Aquaporins of Man and Animals: Basic and Clinical Aspects. Belaruskaya Nauka Publishing House, Minsk, Belarus.

69. Titovets E, Nechipurenko N, Griboedova T, Vlasyuk P (2000) Experimental study on brain oxygenation in relation to tissue water redistribution and brain oedema. Acta Neurochir Suppl 76: 279-81.

70. Titovets E, Stepanova T (2004) Conceptual mathematical model for convective mechanism of brain cortex oxygenation. News of Biomed Sci 2: 127-34.

71. Thompson JK, Peterson MR, Freeman RD (2003) Single-neuron activity and tissue oxygenation in the cerebral cortex. Sci 299: 1070-2.

72. Ivanov A, Zilberter Y (2011) Critical state of energy metabolism in brain slices: the principal role of oxygen delivery and energy substrates in shaping neuronal activity. Front Neuroenerg 3: 9.

73. Sugano T, Oshino N, Chance B (1974) Mitochondrial functions under hypoxic conditions: The steady states of cytochrome c reduction and of energy metabolism. BBA 347: 340-58.

74. Chance B, Cohen P, Jobsis F, Schoener B (1962) Intracellular Oxidation-Reduction States in Vivo: The microfluorometry of pyridine nucleotide gives a continuous measurement of the oxidation state. Sci 137: 499-508.

75. Titovets E (1987) Membrane Open-System Cell for Oxygen Consumption Measurement. Anal Biochem 166: 79-82.

76. Titovets E, Parkhach L, Stepanova T, Matusevich L (2009) [Study of the Mechanism of Oxygen Metabolism in Human Red Blood Cells] Russian. Biofisika 10: 425-41.

77. Titovets E, Koshkin V, Parhach L (2005) Oxygen flux control of mitochondrial respiration and energy function. News of Biom Sci 1: 5-13.

78. Thrane AS, Takano T, Thrane VR, Wang F, Peng W, et al. (2013) In vivo NADH fluorescence imaging indicates effect of aquaporin-4 deletion on oxygen microdistribution in cortical spreading depression. J Cereb Blood Flow Metab 33: 996-9.

79. Torre F, Rodriguez-Baeza A, Sahuquillo-Barris J (1998) Morphological Characteristics andDistribution Pattern of the ArterialVessels in Human Cerebral Cortex: A Scanning Electron Microscope Study. The Anatomical Record 251: 87-96.

80. Tsai AG, Johnson PC, Intaglietta M (2003) Oxygen Gradients in the Microcirculation. Physiol Rev 83: 933-63.